Journal of Magnetic Resonance **142,** 241–253 (2000)
doi:10.1006/jmre.1999.1936, available online at http://www.idealibrary.com on IDEAL®

A Fast Variant of ^{1}H Spectroscopic U-FLARE Imaging Using Adjusted Chemical Shift Phase Encoding

Andreas Ebel,[1] Wolfgang Dreher, and Dieter Leibfritz

Universität Bremen, Fachbereich 2 (Chemie), Leobener Strasse, 28334 Bremen, Germany

Received April 7, 1999; revised August 4, 1999

So far, fast spectroscopic imaging (SI) using the U-FLARE sequence has provided metabolic maps indirectly via Fourier transformation (FT) along the chemical shift (CS) dimension and subsequent peak integration. However, a large number of CS encoding steps N_ω is needed to cover the spectral bandwidth and to achieve sufficient spectral resolution for peak integration even if the number of resonance lines is small compared to N_ω and even if only metabolic images are of interest and not the spectra in each voxel. Other reconstruction algorithms require extensive prior knowledge, starting values, and/or model functions. An adjusted CS phase encoding scheme (APE) can be used to overcome these drawbacks. It incorporates prior knowledge only about the resonance frequencies present in the sample. Thus, N_ω can be reduced by a factor of 4 for many ^{1}H *in vivo* studies while no spectra have to be reconstructed, and no additional user interaction, prior knowledge, starting values, or model function are required. Phantom measurements and *in vivo* experiments on rat brain have been performed at 4.7 T to test the feasibility of the method for proton SI.

Key Words: **adjusted chemical shift phase encoding; U-FLARE; proton NMR spectroscopic imaging; rat brain.**

INTRODUCTION

In multidimensional SI, the conventional approach of acquiring N_ω data points in the CS dimension k_ω in combination with multiple phase encoding gradients to traverse k-space along orthogonal axes k_x, k_y, and k_z (*1, 2*) leads to unacceptably long minimum total measuring times $T_m = N_x \cdot N_y \cdot N_z \cdot TR$. Alternatives have been proposed to overcome this problem (*3–10*). Spectroscopic U-FLARE (*10*) makes use of the fact that long T_1 and T_2 relaxation times of proton metabolites (*11*) allow multiple spin-echo acquisition after a single excitation. Moreover, the echoes do not suffer from dephasing due to J modulation, provided the inverse of the delay ΔTE between subsequent echoes is large compared to the chemical shift difference $\Delta\delta$ of coupled nuclei and their coupling constants J (in Hz) (*12, 13*). Recently, proton spectroscopic U-FLARE imaging has been demonstrated to be capable of measuring not only uncoupled or intense weakly coupled signals but also strongly coupled resonances such as glutamate (Glu), glutamine (Gln), *myo*-inositol (Ins), taurine (Tau), or N-acetylaspartate (NAA) (*14*). Using the sliced k-space approach (*4*), $N_x \times N_y$ data points are acquired per excitation, while the chemical shift is encoded within the constant time (CT) evolution period (*15*): The delay tc between excitation and the start of the U-FLARE sequence is kept constant, the position of a refocusing pulse is changed between subsequent excitations (see Fig. 1a), and a pseudo-echo in k_ω is acquired. Thus, the minimum total measuring time is $T_m = N_\omega \cdot N_z \cdot TR$. Note that shifting the pulse position by an increment $\Delta\tau/2$ will shift the position of the refocused spin-echo by $\Delta\tau$. As known from single voxel studies (*16*), this encoding technique provides better signal separation because of effective homonuclear decoupling, but also leads to a strong dependence of the signal intensities of coupled resonances on tc and the coupling pattern.

Until now, the number of CS encoding steps N_ω and the increments $\Delta\tau_j$ ($j = 0, \ldots, N_\omega - 1$), by which the echo position is shifted, have been chosen to satisfy the following conditions:

1. To reconstruct spectra by means of standard fast Fourier transform (FFT) algorithms (*17, 18*), the pseudo-echo in k_ω must be acquired at equidistant sampling intervals leading to a constant increment $\Delta\tau_j \equiv \Delta\tau = const$. For a signal sampled at equidistant intervals, the sampling theorem (*19*) implies that the sampling interval must not be greater than $1/SW$ to cover the spectral bandwidth SW (in Hz) completely.
2. The range of encoding times $T_t := (N_\omega - 1)|\Delta\tau|$ must be long enough to provide sufficient spectral resolution $\delta\nu = 1/T_t$ (in Hz). This, in turn, requires a sufficiently large number of CS encoding steps N_ω and a sufficiently long evolution period tc.

In summary, N_ω is usually chosen to be the smallest integer greater than the ratio $SW/\delta\nu$. In principle, the spectral resolution $\delta\nu$ should be considerably smaller than the separation of adjacent spectral lines to allow unambiguous identification of metabolite resonances and accurate determination of peak areas. Note that line splittings due to J coupling need not be

[1] Present address: University of California San Francisco and VA Medical Center, MRS Unit, 4150 Clement St. (114M), San Francisco, CA 94121.

1090-7807/00 $35.00

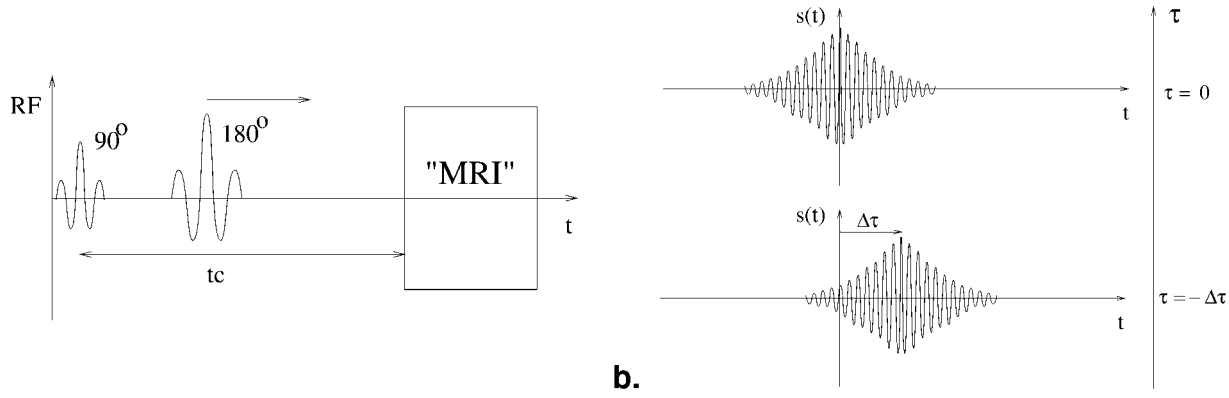

FIG. 1. (a) Schematic pulse sequence for an experiment using CT chemical shift phase encoding: After excitation the refocusing pulse is shifted as indicated by the arrow while the delay *tc* between excitation and the imaging sequence is kept constant. (b) Schematic illustration of how to determine the sign of CS encoding times: At the top, the completely refocused spin-echo is sampled corresponding to $\tau = 0$ s. At the bottom, the echo has been shifted "to the right" by an increment of magnitude $\Delta\tau$. As indicated at the vertical axis denoting the CS phase encoding direction τ, this shift corresponds to a negative encoding time.

considered because of the effective homonuclear decoupling. However, the range of encoding times T_t is limited due to the rapid decay of the pseudo-echo in k_ω caused by B_0 inhomogeneities. Any substantial increase of T_t (corresponding to a decrease of $\delta\nu$) would cause additional noise contamination of the spectra. Under the experimental conditions of this study, i.e., $B_0 = 4.7$ T, a spectral resolution on the order of 15 Hz can be achieved using $SW = 900$ Hz (4.5 ppm) and $N_\omega = 64$ (*14*).

This procedure will be termed "conventional" in the following. It provides metabolic maps by FT with respect to the equidistantly sampled CS direction and subsequent peak integration and implies a few disadvantages:

1. While SI applications with 2D spatial/1D spectral resolution can be carried out within a sufficiently short minimum total measuring time (*14*), extensions aiming at 3D spatial maps of CS information or at 2D spatial/2D spectral experiments would still be too long for clinical applications.
2. Furthermore, proton NMR spectra are sparsely populated with strong resonance lines: large spectral intervals contain noise and no or only little metabolite information. As for many applications it is known a priori which spectral intervals are of interest, it is desirable to apply a sampling method that avoids collecting data corresponding to signal-free spectral regions (*20*).

Therefore, a reduction of the minimum total measuring time is not only *necessary* for advanced applications of spectroscopic U-FLARE imaging, it is also *possible* because it follows from the second statement that the conventional procedure mathematically leads to a solution of a strongly overdetermined system of equations. Alternative reconstruction methods, e.g., VARPRO (*21*) or HLSVD (*22*) processing the data in the time domain, require extensive prior knowledge, starting values, and/or model functions. Frequency domain techniques, e.g., line shape fitting models (*23, 24*), depend on the availability of data that can be processed by FT and are thus restricted in the same way as the conventional CS phase encoding and reconstruction procedure for spectroscopic U-FLARE. In this study, we will present an alternative sampling/reconstruction scheme to overcome these drawbacks. The method exploits prior knowledge about the resonances present in the sample and leads to a considerable reduction of the minimum total measuring time. This reduction is achieved retaining information about all resonances in contrast to soft-COSY (*25*) or related techniques. These use spectrum simplification by chemical shift selective RF pulses to suppress certain parts of the spectrum.

METHODS

Theory of Adjusted Chemical Shift Phase Encoding (APE)

The experiment schematically shown in Fig. 1a leads to a signal, which for one CS phase encoding step with index j represented by an encoding time τ_j can be described as

$$s_j := s(\tau_j) = \sum_{k=0}^{K-1} m_k \exp(i\omega_k\tau_j)\, f(\tau_j). \qquad [1]$$

The N_ω complex-valued CS phase encoded signals s_j as well as the K complex-valued signals m_k of individual metabolite resonances with frequencies ω_k may be functions of spatial and/or spectral coordinates depending on the experiment carried out after the evolution period tc. The module labelled "MRI" in Fig. 1a represents a 2D or 3D U-FLARE sequence, for example, or it may be simply replaced by immediate spin-echo acquisition (see below). The signals m_k depend on the time constant tc as well as on the corresponding relaxation times $T_{2,k}$ and $T_{1,k}$ and in the case of coupled resonances on the coupling constants J_k. The complex-valued function f in Eq. [1] represents the effect of B_0 inhomogeneities, i.e., the signal

attenuation due to dephasing as well as the local shift of resonance frequencies. Note that the function f is independent of the resonance index k for signals m_k originating from a sufficiently small or homogeneous volume within the sample. Its magnitude can often be described by an exponential function $|f(\tau_j)| \approx \exp(-|\tau_j|/T_2^{**})$ with the effective decay time T_2^{**} *due to* B_0 inhomogeneities. An encoding time $\tau_j = 0$ s corresponds to a completely refocused spin-echo with $f(\tau_j = 0 \text{ s}) \equiv 1$. In the absence of B_0 inhomogeneities and for the special case of N_ω equidistant samples s_j as well as $K = N_\omega$ equidistant frequencies ω_k, the sum in Eq. [1] is equivalent to the discrete FT of a signal represented by its Fourier coefficients m_k. It is important to note that the sign of τ_j depends on which side the pseudo-echo in k_ω is sampled with respect to its maximum. Increasing (decreasing) the delay between the 90° and 180° pulses in Fig. 1a corresponds to a "right" ("left") shift of the echo position and implies sampling the echo "before" ("after") its maximum, i.e., at $\tau_j < 0$ s ($\tau_j > 0$ s), as is schematically shown in Fig. 1b for simple spin-echo acquisition.

The problem to solve the set of N_ω equations given by Eq. [1] for the K unknown signals m_k with $K \leq N_\omega$ turns out to be a linear least squares problem, which in matrix notation can be expressed as

$$\begin{aligned} &s = FAm \\ &\text{with } s := (s_0, s_1, \ldots, s_{N_\omega - 1})^\dagger \\ &\text{and } m := (m_0, m_1, \ldots, m_{K-1})^\dagger, \end{aligned} \qquad [2]$$

where the symbol "†" denotes transposition. The $N_\omega \times N_\omega$ diagonal matrix F is defined by $F_{jk} := \delta_{jk}|f(\tau_j)|$ and represents the amplitude attenuation due to B_0 inhomogeneities. If the latter are related to the efficient decay time T_2^{**} and provided that the generalized range of encoding times $T_t := \max_j(\tau_j) - \min_j(\tau_j) \ll T_2^{**}$, F may be replaced by the unity matrix. Furthermore, the $N_\omega \times K$ matrix A represents the phase factors $A_{jk} := \exp[i(\omega_k + \Delta\omega_B)\tau_j]$ incorporating the frequency shift $\Delta\omega_B$ due to field inhomogeneities. It has been pointed out earlier (*20*) that if the K resonance frequencies ω_k were known it would be sufficient, in principle, to provide $N_\omega = K$ signals s_j to solve Eq. [2]. The only restriction on the choice of CS phase encoding times would be the necessity of a nonsingular matrix $B := FA$. We will show, however, that using $N_\omega > K$ renders the solution more robust. In this general case, the least squares solution to Eq. [2] can be written as

$$m = B^+ s \equiv A^+ F^{-1} s, \qquad [3]$$

provided A is nonsingular. The $K \times N_\omega$ matrix A^+ is the pseudo-inverse (*26*) of the phase matrix A with $A^+ = (A^H A)^{-1} A^H$. Here, A^H denotes the Hermitian conjugate of A with $A_{kj}^H = \exp[-i(\omega_k + \Delta\omega_B)\tau_j] \equiv A_{jk}^*$. The matrix inverse F^{-1} exists because the real-valued diagonal elements of F are always greater than zero, and it is given by $F_{jk}^{-1} = \delta_{jk}|f(\tau_j)|^{-1}$. The calculation of m by Eq. [3] will be referred to as the "APE reconstruction" in contrast to the conventional reconstruction mentioned earlier.

An early application of the APE procedure is the Dixon method for the separation of water and fat (*27*): Knowing the MRI signal consists of contributions from water and fat only and supplying their chemical shifts ω_0 and ω_1, respectively, as prior knowledge, the two phase-encoded signals $s_0 \equiv s(\tau_0 = 0 \text{ s})$ and $s_1 \equiv s(\tau_1 = \pi/(\omega_0 - \omega_1))$ can be used to calculate the individual signals m_0 (for water) and m_1 (for fat) from Eq. [3]. The value of τ_1 is chosen so that the two resonances develop a phase difference of 180°, which simplifies the reconstruction as it amounts to adding/subtracting the signals s_0 and s_1. However, if uncorrected, different attenuation of the two signals due to B_0 inhomogeneities as well as the frequency shift $\Delta\omega_B$ will lead to reconstruction errors (*28*).

To implement the APE method outlined above, two problems must be considered:

1. The number N_ω and the values of the CS phase encoding times τ_j must be chosen appropriately to set up the experiment.
2. The influence of B_0 inhomogeneities, i.e., the frequency shift $\Delta\omega_B$ as well as the attenuation factors $|f(\tau_j)|$ must be determined to reconstruct metabolite signals.

The Choice of CS Phase Encoding Times

Provided $N_\omega \geq K$ is obeyed, the encoding times τ_j may be chosen arbitrarily, in principle, with no restriction on their respective differences as long as the nonsingularity of matrix A is maintained. However, a major problem of spectroscopic U-FLARE as of most NMR experiments is the contamination of the measured signals s_j by random noise. The choice of encoding times should therefore aim to reduce the noise in the spectroscopic images that will be reconstructed by the APE method. From the general theory of linear least squares problems (*29*) it is known that the covariance matrix of m is given by

$$V(m) = \sigma^2 (B^H B)^{-1} \equiv \sigma^2 B^+ B^{+H}. \qquad [4]$$

Here, σ denotes the standard deviation of random noise in the signals s_j. From Eq. [4] it follows that the standard deviation of noise in the reconstructed signal m_k will be

$$\sigma(m_k) = \sqrt{\sum_{j=0}^{N_\omega - 1} |B_{kj}^+|^2} \cdot \sigma \equiv \|B^+\|_k \cdot \sigma, \qquad [5]$$

where $\|B^+\|_k$ is the Euclidean norm of the kth row vector of matrix B^+. To find a quantity that incorporates the influence of

TABLE 1
Values of $\|B^+\|_k$ Calculated According to Eq. [5] for Different Choices of N_ω[a]

		N_ω					
Metabolite	(δ [ppm])	8	10	12	14	16	Optimized $N_\omega = 16$
H_2O	(4.70)	0.562	**4.52**	**0.665**	0.315	0.292	**0.325**
PCr	(3.93)	0.717	0.389	0.345	0.315	0.295	0.302
Ins	(3.62)	**4.62**	0.378	0.343	0.314	0.294	0.306
Cho	(3.24)	0.644	0.421	0.382	**0.354**	**0.331**	**0.325**
PCr	(3.04)	0.673	0.421	0.382	0.352	0.330	**0.325**
Glu	(2.36)	0.535	0.394	0.342	0.314	0.293	0.310
NAA	(2.02)	0.677	4.51	0.346	0.313	0.293	0.320
Lip	(1.50)	4.61	0.391	0.663	0.314	0.292	0.311
$\|B^+\|_{\min}$		0.414	0.369	0.336	0.310	0.290	0.292
$\Delta\tau$ [ms]		−2.383	−1.853	−1.516	−1.283	−1.112	—

[a] Calculations are based on metabolite resonances visible at $TE = 136$ ms *in vivo* with $B_0 = 4.7$ T, $T_2^{**} = 30$ ms, and $T_t := (N_\omega - 1)|\Delta\tau| = 16.68$ ms. All encoding schemes except the optimized scheme are equidistant, and the sampling times are assumed to be centered with respect to the maximum of the pseudo-echo in k_ω. The value of $\|B^+\| \equiv \max_k(\|B^+\|_k)$ is printed in boldface.

noise on *all* components of m we define the matrix norm of B^+ by

$$\|B^+\| := \max_k(\|B^+\|_k). \qquad [6]$$

From the definition of $\|B^+\|$ it follows that its value is independent of any global frequency shift such as that due to field inhomogeneities, $\Delta\omega_B$ (*30*). A more empirical description of the propagation of noise has been given earlier (*31*), and it was shown that minimizing a function similar to $\|B^+\|$ considerably enhances the robustness of the solution [3].

Returning to the example given by the Dixon method and neglecting the influence of field inhomogeneities for the present ($B \approx A$), it is easy to see that the phase matrix A is given by

$$A = \begin{pmatrix} 1 & 1 \\ e_0 & e_1 \end{pmatrix}$$

and its pseudo-inverse is

$$A^+ = \frac{1}{(e_1 - e_0)} \begin{pmatrix} e_1 & -1 \\ -e_0 & 1 \end{pmatrix}, \qquad [7]$$

with the abbreviation $e_n := \exp(i\omega_n\tau_1)$ for $n = 0, 1$. It is straightforward to show that $\|A^+\| = \sqrt{2}/|e_1 - e_0|$ and that this quantity will reach a minimum if $e_0/e_1 = -1$. This corresponds to $\tau_1 = (2n + 1)\pi/(\omega_0 - \omega_1)$ with $n \in \mathbb{N}$, which suggests the value $\tau_1 = \pi/(\omega_0 - \omega_1)$ should be chosen to satisfy $T_t \equiv \tau_1 \ll T_2^{**}$. Thus, the Dixon method is a special case of the APE method using optimized phase encoding times corresponding to a minimum of $\|B^+\|$. Note that for the Dixon method $\|B^+\| = 1/\sqrt{2}$.

In the more general case with $K > 2$ signals to be reconstructed, the minimization of $\|B^+\|$ implies an optimization of N_ω CS phase encoding times, which is a nontrivial numerical problem because the probability of being trapped in local minima increases with increasing N_ω. Moreover, the optimization is hampered by the fact that the dependence of the attenuation factors $|f(\tau_j)|$ on the encoding times τ_j is a priori unknown. An approximation could be given assuming that the pseudo-echo in k_ω decays exponentially, $|f(\tau_j)| \approx \exp(-|\tau_j|/T_2^{**})$. There exists a lower limit on $\|B^+\|$ given by (*30*)

$$\|B^+\|_{\min} = \frac{1}{\sqrt{\sum_{j=0}^{N_\omega - 1} |f(\tau_j)|^2}}. \qquad [8]$$

If B_0 inhomogeneities can be neglected, all the terms in the sum are approximately equal to 1, and the limit becomes $\|B^+\|_{\min} = 1/\sqrt{N_\omega}$, which has already been verified for the Dixon method. Then, noise is propagated from the experimental signals s into the reconstructed signals m as by peak integration in the case of an "ideal spectrum" where each peak (shaped like a Dirac delta function) is located at a single spectral coordinate and its intensity is determined by a "one-point" integration.

To allow a comparison of both CS phase encoding/reconstruction methods using the same experimental data, it is necessary to choose a subset of N_ω out of a total of $N_{\omega 0}$ equidistant samples. Although one is not forced to choose an equidistant subset to perform the APE reconstruction, we found that if N_ω is sufficiently greater than the number of resonances K, the norm of matrix B^+ is only insignificantly greater than its lower limit given by Eq. [8]: Table 1 gives a numerical demonstration of how the value of $\|B^+\|$ (and of all $\|B^+\|_k$) depends on the number of samples for a fixed set of

$K = 8$ resonances typically visible in the *in vivo* experiments at 4.7 T of this study. The resonance frequencies of these metabolites were provided as prior knowledge assuming that the temperature-dependent chemical shift of water is 4.70 ppm. Each value of $\|B^+\|_k$ was calculated according to Eq. [5] for $N_\omega = 8$, 10, 12, 14, and 16 assuming exponentially decaying amplitudes with $T_2^{**} = 30$ ms, which was observed in the data on average. In each case the same range of encoding times $T_t = 16.68$ ms was divided into $N_\omega - 1$ intervals of equal length $\Delta\tau$. This value of T_t will be discussed in the Experimental section. It can be seen that the maximum of $\|B^+\|_k$ (printed in boldface in Table 1) is decreasing with increasing N_ω and that it approaches its theoretical lower limit, which was calculated according to Eq. [8]. The tendency of the norms $\|B^+\|_k$ to converge at $\|B^+\|_{\min}$ with increasing N_ω is also visible. The last column of Table 1 contains the values of $\|B^+\|_k$ obtained under the same conditions after performing a numerical optimization for $N_\omega = 16$. The following CS encoding times (in ms) were found to lead to a (local) minimum of $\|B^+\|$ using a simplex minimization algorithm (*32*):

$$\begin{aligned}\tau = (&-8.394, -7.074, -6.372, -5.005, -4.420,\\ &-3.477, -2.247, -1.374, 0.395, 2.016, 2.863,\\ &4.262, 4.711, 5.922, 6.965, 8.240).\end{aligned}$$

We conclude that choosing $N_\omega = 16$ equidistant CS phase encoding times from the set of $N_{\omega 0} = 64$ samples conventionally used for proton spectroscopic U-FLARE will allow nearly optimal noise propagation for the APE reconstruction method while it still leads to a reduction of the minimum total measuring time T_m by a factor of 4. In the experiments of this study, $N_\omega = 16$ will always satisfy the condition $N_\omega \geq K$ necessary for solving Eq. [2]. As the chemical shift of water must be supplied to set up the prior knowledge for the APE algorithm, it must be determined, e.g., by measuring the frequency difference between the signals of water and NAA (2.02 ppm) (*33*) in a spectrum acquired with an additional single voxel experiment. Furthermore, successful application of the APE method requires temperature variations across the sample to be negligible.

Treatment of B_0 Inhomogeneities

After the CS encoding times have been chosen and the experiment has been performed, the twofold influence of B_0 inhomogeneities must be taken into account before the reconstruction of metabolite signals m according to Eq. [3] is possible:

1. The frequency shift $\Delta\omega_B$ must be determined for each voxel to set up the $N_\omega \times K$ phase matrix A according to $A_{jk} = \exp[i(\omega_k + \Delta\omega_B)\tau_j]$.
2. The N_ω attenuation factors $|f(\tau_j)|$ must be provided for each voxel to account for the decay of signal amplitudes.

Both effects can be addressed using a water reference measurement performed under the same conditions as the experiment used to obtain the signals s_j except for the water suppression (*34–37*). Neglecting noise contamination, the water reference signal can be expressed as

$$r_j := r(\tau_j) = r_W \exp(i\phi_W)\exp[i(\omega_W + \Delta\omega_B)\tau_j]|f(\tau_j)|, \quad [9]$$

with amplitude r_W, phase ϕ_W, and frequency ω_W. For the resonant water signal with $\omega_W/2\pi = 0$ Hz, the phase of the reference signal is given by

$$\phi(\tau_j) = \phi_W + \Delta\omega_B\tau_j. \quad [10]$$

As ϕ is unique within the range $0 \leq \phi < 2\pi$, it must be corrected for cyclic "wrap around" at these limits. Equation [10] allows the determination of $\Delta\omega_B$ by linear regression, which is very accurate (*30*) as well as computationally more efficient than spectral peak picking because no zero filling followed by FT of the inflated data must be performed. Moreover, for the APE method, FT and peak picking may not be possible because the CS encoding times do not necessarily satisfy the sampling theorem.

The attenuation factors $|f(\tau_j)|$ can be determined from Eq. [9] by dividing the magnitude of the reference signal by its maximum value:

$$|f(\tau_j)| = \frac{|r(\tau_j)|}{\max_n[|r(\tau_n)|]}, \quad [11]$$

which implies normalization to an arbitrary scale.

EXPERIMENTAL

Hardware and Pulse Sequence

The pulse sequence used is shown in Fig. 2. It is derived from the improved spectroscopic U-FLARE sequence proposed by (*14*) and has been implemented on our 4.7 T/40 cm Bruker Biospec system (Bruker Medizintechnik GmbH, Karlsruhe, Germany). This is equipped with self-shielded gradients of inner diameter 200 mm, capable of switching 170 mT/m in 450 μs. RF pulse transmission was accomplished using a 98-mm diameter saddle-type resonator, which for phantom measurements was also used for signal detection. Spectroscopic images were obtained in coronal slice orientation *in vivo* from the brains of healthy 400-g male Wistar rats anaesthetized with 0.8–1.5% halothane in 7:3 N_2O:O_2. An 18-mm diameter surface coil placed directly above the head of the rat was used for signal reception. The phantom consisted of 7 cylindrical tubes of 5 mm diameter filled with aqueous solutions of *myo*-inositol (Ins, 100 mM), phosphocreatine (PCr, 80 mM), glutamate (Glu, 77 mM), N-acetyl-aspartate

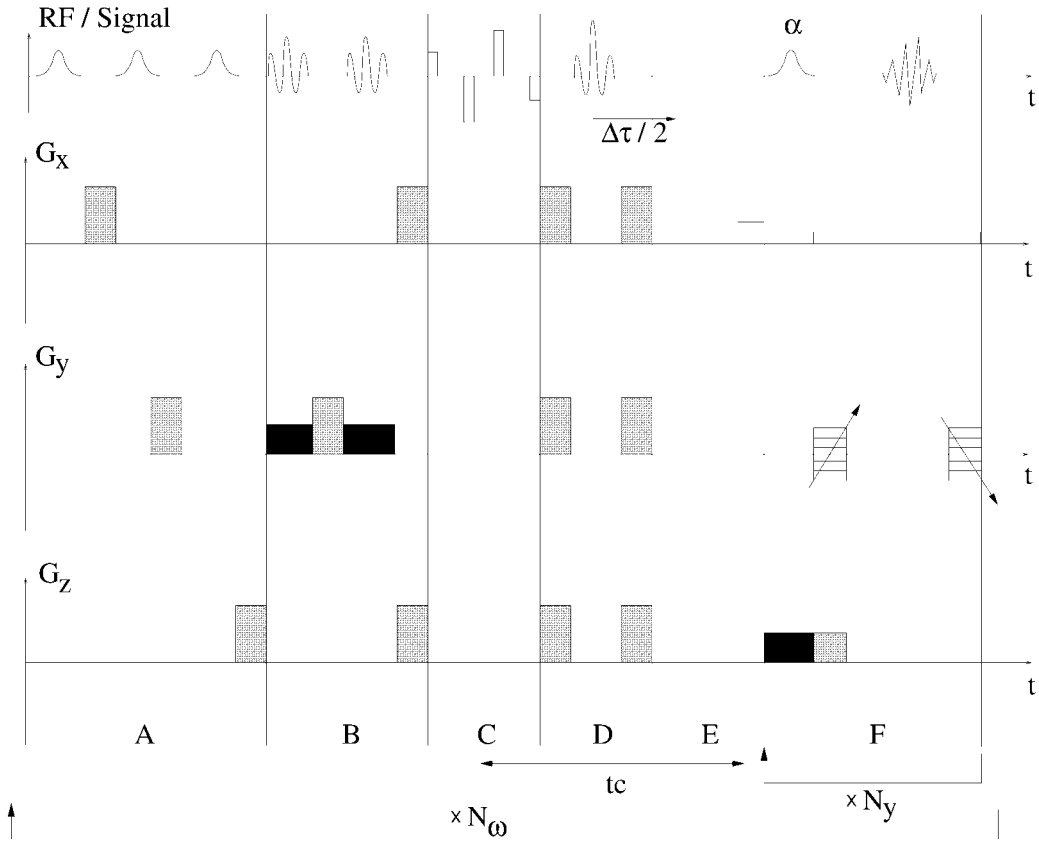

FIG. 2. Pulse sequence for displaced spectroscopic U-FLARE. The gray shaded gradient pulses are spoilers, whereas those filled with black (white) are slice (phase) gradients. The sequence is divided schematically into six parts: (A) frequency selective water presaturation; (B) spatially selective lipid presaturation; (C) frequency selective excitation; (D) and (E) CS phase encoding and evolution period; (F) U-FLARE imaging sequence.

(NAA, 57 mM), glutamine (Gln, 29 mM), taurine (Tau, 19 mM), and choline chloride (Cho, 14 mM), respectively. These tubes were inserted into a test tube of 28 mm diameter filled with water. All metabolite concentrations were chosen to provide ratios that mimic the *in vivo* situation (*38*). Spectroscopic images of the phantom were obtained from slices perpendicular to the cylinder axis.

Water presaturation was performed using three consecutive Gaussian RF pulses of 15 ms duration (FWHM-bandwidth 166 Hz) followed by spoiler gradients (Fig. 2, part A). For the *in vivo* experiments, two 90° RF pulses with optimized sinc-like shape (*39*) were used for spatially selective lipid presaturation. The slice gradients and transmitter frequency offset were adjusted to achieve minimum signal from outside the skull (part B). Frequency selective excitation was performed using the hard pulse sequence $1 - 2\tau - \overline{5.4} - \tau - 5.4 - 2\tau - \bar{1}$ (*40*) with $\tau = 1.25$ ms and an effective flip angle of 79.2°. In the evolution period (parts D and E) the position of an optimized 180° refocusing pulse (*41*) of 2.5 ms duration was shifted with respect to the excitation pulse and the start of the U-FLARE imaging sequence, while the delay *tc* between these two was kept constant (cf. Fig. 1a). The gradient in part E was used for preparation of the phase encoding in the readout direction k_x. Part F represents one ΔTE period of the U-FLARE sequence. A slice selective Gaussian pulse of 300 μs duration with a flip angle of $\alpha = 135°$ was used for refocusing the echoes, which were acquired under a constant readout gradient after phase encoding along k_y. The readout gradient was switched on 750 μs before the acquisition to support the separation of even and odd echoes (*42*). Only the even echoes were acquired (displaced variant of U-FLARE). The spoiler immediately following the slice gradient also contributed to the separation of the echoes and served to destroy unwanted FID/SSFP signals arising directly from the refocusing pulses. Part F was repeated 38 times in all: Six dummy cycles were performed without either signal acquisition or phase encoding gradient before the signal was acquired 32 times using the alternate phase encoding scheme (*43*) for k_y. Four complete dummy experiments were performed without signal acquisition to reach dynamic equilibrium.

A matrix of 32×32 complex data points was acquired after one excitation at a readout bandwidth of 10 kHz and an echo separation of $\Delta TE = 5$ ms. Although this delay between subsequent echoes does not satisfy the condition $\Delta TE^{-1} \gg \Delta\delta$, J (in Hz) for some ^{1}H metabolite signals, no deleterious effect due to J modulation was observed in the experiments. CS

phase encoding was performed at $tc = 136$ ms to detect signals from coupled resonances of Glu and Ins (*14*). The position of the refocusing pulse in part D of the sequence was shifted in $N_{\omega 0} = 64$ steps of $\Delta\tau/2 = -556$ μs corresponding to a spectral bandwidth of 899 Hz and giving rise to pseudo-echoes in k_ω. The phase encoding steps were chosen to sample the pseudo-echo symmetrically around its maximum. With a field of view (FOV) of 48×48 mm^2 and a slice thickness of 3 mm the nominal voxel size was $1.5 \times 1.5 \times 3$ mm^3. Two experiments were accumulated, and four identical repetitions were performed for subsequent image reconstruction with both the conventional and the APE method. With $TR = 1.9$ s the measuring time per repetition was approximately 4 min. The same experiment was then repeated only once without water suppression to obtain the water reference signal. The resonance frequency of water was adjusted to $\omega_W/2\pi = -400$ Hz ($\triangleq$ 2.7 ppm *in vivo*) to avoid signal loss by frequency selective excitation.

Data Processing and Evaluation

For the conventional reconstruction of spectroscopic U-FLARE images, the complex data set of dimensions $32 \times 32 \times 64$ ($N_x \times N_y \times N_{\omega 0}$) was processed using the Interactive Data Language (IDL, Research Systems, Inc., Boulder, CO) (*44*) according to the following protocol:

1. DC correction in k_ω,
2. spatial apodization using a standard Hamming window,
3. CS apodization using a sine-bell window,
4. zero filling in k_ω to 256 complex points and 3D FFT,
5. interactive definition of spectral intervals of interest (width: 5 to 6 points),
6. correction of the position of these intervals for the frequency shifts $\Delta\omega_B$ due to B_0 inhomogeneities; the shifts were determined from the water reference signal according to Eq. [10],
7. peak integration inside the corrected intervals,
8. FT interpolation "$(N_x, N_y) \rightarrow (64, 64)$."

For the calculation of spectroscopic images using the APE method we employed a combination of IDL and C routines and made use of the LAPACK library (Linear Algebra Package) (*45*). While steps 1 and 2 were the same as above, the following protocol was executed:

3. Selection of $N_\omega = 16$ CS phase encoding steps out of the total of $N_{\omega 0} = 64$ (see below),
4. accumulation of four repetitions of the experiment to provide the same total measuring time as for the conventional reconstruction,
5. FFT with respect to k_x and k_y,
6. correction for amplitude attenuation due to field inhomogeneities according to Eq. [11],
7. set up of the array of resonance frequencies ω_k for all K signals to be expected and correction for the frequency shifts $\Delta\omega_B$,
8. calculation of magnitude signals $|m_k|$ using Eq. [3],
9. FT interpolation "$(N_x, N_y) \rightarrow (64, 64)$."

The main resonances ($K = 7$) to be expected for the phantom at $tc = 136$ ms were NAA (CH_3, 2.02 ppm), PCr (CH_2, 3.93 ppm and CH_3, 3.04 ppm), Cho ($N(CH_3)_3$, 3.24 ppm), Ins ([4, 6]CH, 3.62 ppm), Glu (γCH_2, 2.36 ppm), and water (4.88 ppm). Other signals of NAA were not detected because of signal attenuation due to the frequency selective excitation sequence applied (αCH, 4.40 ppm) and due to the small values of their transfer functions at $tc = 136$ ms (βCH, 2.52 ppm and β'CH, 2.70 ppm). The same applies to other signals of Ins ([1, 3]CH, 3.54 ppm, [2]CH, 4.06 ppm, and [5]CH, 3.28 ppm), some of which are visible but too small (compared with the noise level) to be used for reconstructing spectroscopic images. This also holds for other signals of Glu (αCH, 3.76 ppm, βCH, 2.06 ppm, and β'CH, 2.10 ppm). Signals of Gln and Tau were not detected in our experiments because of the low metabolite concentrations and the transfer functions of the coupled resonances (see next section). Disregarding signals of Gln and Tau—as was also done for the numerical demonstration in Table 1—enhanced the robustness of the APE algorithm as the ratio N_ω/K was increased. The chemical shift of water was obtained from the conventional spectra; no significant variations across the slice in the phantom or in the rat brain were observed.

For the *in vivo* data, the chemical shift of water was 4.70 ppm, and a broad lipid signal (Lip) due to imperfect presaturation was identified at 1.3 ppm. Furthermore, the label Cho reflects choline containing compounds *in vivo*, and Cr + PCr stands for total creatine. As Glu and Gln will not be resolved, their common signal will be referred to as Glx. The signals of Ins at 3.62 and 3.54 ppm were not resolved *in vivo*. The resonance at 3.62 ppm was dominant for $tc = 136$ ms. Therefore, this chemical shift was chosen for the APE reconstruction. Thus, in addition to the 7 resonances considered for the phantom measurements, consideration of the lipid signal led to $K = 8$ resonances to be reconstructed from the *in vivo* data.

To choose 16 CS phase-encoding times was based on the purpose of minimizing the value of $\|B^+\|$. As the shape of the pseudo-echo in k_ω and thus the matrix of attenuation factors F varied across the sample, a unique choice could not be optimal for all voxels simultaneously. Moreover, for a general application of the APE method this shape will be unknown in advance. That is why the value of $\|A^+\|$ was used to estimate the robustness of the algorithm. The encoding times were selected as close to the echo maximum as possible because this choice most likely ensures optimal *SNR*. For the phantom data we found that choosing every second CS phase-encoding step ($\Delta\tau_j = \Delta\tau = -2.224$ ms for $j = 0, \ldots, 15$) centered with respect to the echo maximum led to $\|A^+\| = 0.260$, which is

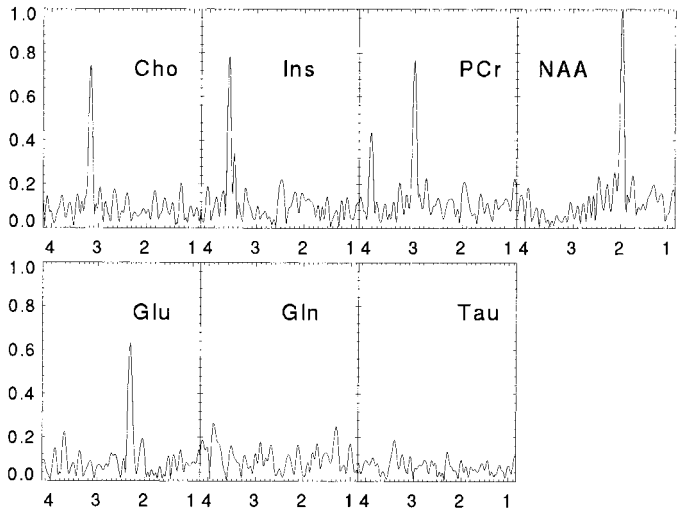

FIG. 3. Typical magnitude spectra acquired from the phantom using the spectroscopic U-FLARE sequence with $tc = 136$ ms. Each spectrum belongs to a voxel inside the tube of the corresponding metabolite and has been normalized to the same (arbitrary) scale. The unit of the chemical shift axis is ppm.

about 4% above the theoretical lower limit $1/\sqrt{N_\omega} = 0.25$. For the *in vivo* data, poorer B_0 homogeneity required the reduction to $\Delta\tau = -1.112$ ms, i.e., every step centered in k_ω. This choice allowed a reconstruction with $\|A^+\| = 0.281$, which is approximately 12% above the lower limit. Note that this choice of $\Delta\tau$ implies that $T_t \equiv (N_\omega - 1)|\Delta\tau| = 16.68$ ms, which was used for the numerical comparisons given in Table 1.

Due to the accumulation of four experiments for APE in step 4, the data set was not exactly the same as the set used for the conventional reconstruction. However, the variation of the conventional results for all four repetitions proved to be negligible compared to noise. Note that step 8, which was performed by calculating the singular value decomposition of the phase matrix A (*26*) with optimized linear algebra software (*45*), had to be carried out only once for the experiment.

RESULTS AND DISCUSSION

Phantom Experiments

The conventional reconstruction required about 17 s on a SUN SPARC20 workstation (SUN Microsystems, Inc., Mountain View, CA), while the APE reconstruction was complete after 6 s. This difference is mainly due to the fact that for the conventional method, the FT must be carried out for 32×32 data sets of 256 complex data points each, while the most time consuming operation of the APE method (step 8), was carried out only once.

Figure 3 shows typical spectroscopic U-FLARE spectra acquired from the phantom. Each magnitude spectrum belongs to a voxel inside the tube of the corresponding metabolite and has been normalized to the same (arbitrary) scale. All signals expected at $tc = 136$ ms are clearly identified except for Gln and Tau whose signal intensities are below the noise level. This is due to the relatively low concentrations of 29 mM for Gln and 19 mM for Tau. Spectroscopic U-FLARE experiments carried out under identical conditions on spherical phantoms filled with solutions of Gln and Tau at concentrations of 50 mM each provided spectra with clearly identifiable signals of both metabolites. These observations verify the choice of resonances, for which images were reconstructed. Furthermore, no significant baseline distortion is visible in these spectra, which means the water suppression is very efficient.

The results of the conventional image reconstruction for the phantom measurements are displayed in Fig. 4. The water image in the top left corner was reconstructed from the unsuppressed water reference signal and shows the array of tubes inside the test tube. The circles in the other images have been overlaid for orientation. These results are to be compared with those obtained by the APE method, which are shown in Fig. 5. Here, the metabolic map in the top left corner shows the reconstruction of the suppressed water signal. In agreement with the quality of water suppression in the spectra of Fig. 3, there is no significant signal visible. The metabolite images are in good agreement with their counterparts of the conventional reconstruction. All tubes can be clearly identified, and noise contaminations appear to be on the same level as in Fig. 4. Minor deviations of tube shapes are due to noise and partial volume effects and may appear enhanced because of the Fourier interpolation.

A quantitative comparison of the results obtained by both reconstruction methods is given in Table 2. For each resonance, the magnitude intensity is given for the voxel of maximum signal. The discrepancy between the two methods is due to the fact that in the conventional approach peak integration was carried out over a limited number of spectral points only. Thus, the integrals do not necessarily provide the total signal intensities. The concentrations c weighted by the number of protons p in each molecular group are given for comparison. They reveal that the ratios of the singlet signals within each reconstruction method are consistent with the expectation. The value of $\|A^+\|_k$ was calculated, to estimate the noise contamination for each metabolite signal according to Eq. [5]. The standard deviations of noise determined from the region outside the phantom provide a measure of accuracy for the intensities $|m_{\mathrm{APE}}|$ and $|m_{\mathrm{CONV}}|$. They also reinforce the impression obtained by visual inspection of the images that both methods provide approximately equal *SNR*. Moreover, there are no significant differences between the noise levels in images of different metabolites, which is reflected by the fact that all values of $\|A^+\|_k$ are approximately equal.

In Vivo Experiments

An MRI image of the healthy rat brain *in vivo* is shown in Fig. 6a, which was acquired from the same slice selected for

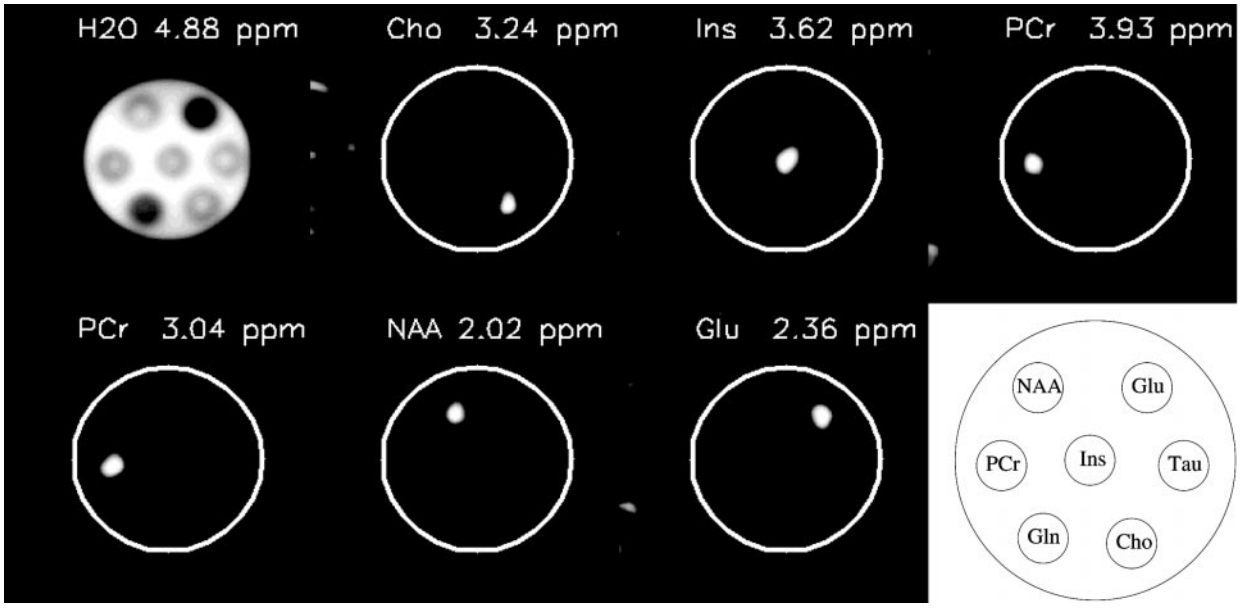

FIG. 4. Spectroscopic U-FLARE images of the phantom obtained by conventional Fourier transform reconstruction and peak integration. The water image in the top left corner was reconstructed from the unsuppressed water reference signal. The circles have been overlaid for orientation. As Gln and Tau could not be detected (cf. Fig. 3), the corresponding images are not shown. In the lower right corner, a schematic representation of the phantom is shown (not to scale).

the spectroscopic U-FLARE experiment. The black square indicates the position of the voxel, for which the magnitude spectrum is shown in Fig. 6b as a typical example. Metabolite assignments correspond to (*46*). Apart from the dominant singlet resonances of NAA, Cr + PCr and Cho, signals from coupled resonances of Glx = Glu + Gln, Ins, and NAA are visible. The Ins resonance at 3.62 ppm is affected by a shoulder due to Glu at 3.76 ppm and Gln at 3.78 ppm. The NAA signals at 2.52 and 2.70 ppm were too small (compared with the noise level) for reconstructing metabolic maps. Signals of Tau were not detected, which is in agreement with its low concentration of 2 mM (*38*) and which corresponds to the results obtained by the phantom measurements (cf. Fig. 3). Recently, however, other authors have reported the detection of Tau with intensi-

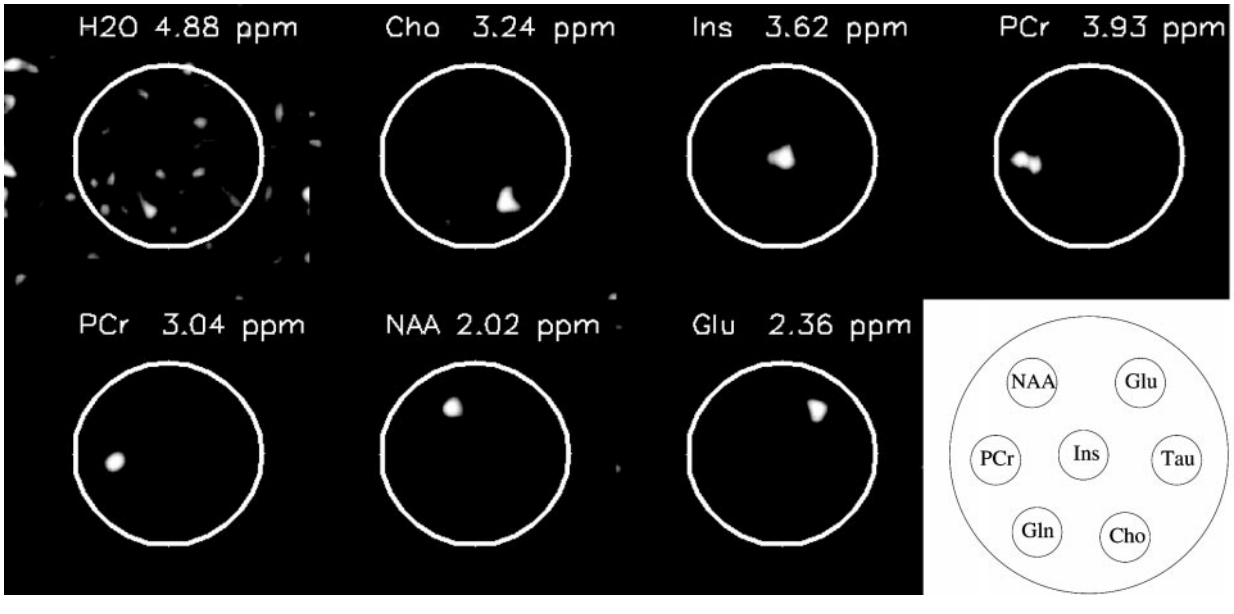

FIG. 5. Metabolic maps of the phantom calculated with the APE algorithm using a selection of 16 out of the total of 64 CS phase encoding steps. The image in the top-left corner shows the reconstruction of the suppressed water signal.

TABLE 2

Comparison of the Results for the Phantom Measurement as Obtained by the APE and the Conventional Reconstruction Method ("CONV")

Metabolite (δ [ppm])	k	$\lvert m_{APE}\rvert$[a] [au]	$\lvert m_{CONV}\rvert$[a] [au]	$c \cdot p$[b] [mM]	$\lVert A^+ \rVert_k$	σ_{APE}[c] [au]	σ_{CONV}[c] [au]
Cho (3.24)	1	54.9	58.7	126	0.260	7.2	8.0
Ins (3.62)	2	65.9	58.3	100	0.253	7.1	6.4
PCr (3.93)	3	67.3	50.1	160	0.254	7.0	7.4
PCr (3.04)	4	97.6	82.3	240	0.258	7.1	6.5
NAA (2.02)	5	85.6	73.7	171	0.256	6.7	7.4
Glu (2.36)	6	61.8	46.5	154	0.253	7.0	6.8

[a] Magnitude signal given for the voxel of maximum intensity inside the corresponding phantom tube.

[b] Product of concentration [mM] and number of protons in the corresponding molecular group.

[c] Standard deviations of the magnitude noise intensities calculated from the region outside the phantom and given in the same (arbitrary) units as the signal intensities.

ties that suggest a higher *in vivo* concentration in the rat brain (*14*, *47*). This matter is currently under investigation.

The spectroscopic U-FLARE images of the rat brain obtained by the conventional method are shown in Fig. 7. As in Fig. 4, the water image in the top-left corner was reconstructed from the unsuppressed water reference signal. All images are restricted to the area of the rat brain as defined by the reference image. These conventional images are to be compared with those reconstructed with the APE algorithm shown in Fig. 8. The water image reconstructed from the data acquired with water suppression shows noise and a small contamination due to lipid signals only. Best consistency between both reconstruction methods is visible for the singlet signals of NAA, Cho, and Cr + PCr (3.04 ppm), whereas the resonances of lower intensity are more severely affected by noise. Among these, the APE images of Glu and Cr + PCr (3.93 ppm) reveal a signal distribution that is more consistent with that of the larger signals than their conventional counterparts. It should be considered that the signal assigned to Glu may also contain a small contribution of Gln. However, as only the chemical shift of the larger signal of Glu at 2.36 ppm was provided as prior knowledge for the APE reconstruction, we termed this signal "Glu."

CONCLUSIONS

We have presented a method for chemical shift phase encoding dedicated to the spectroscopic U-FLARE imaging sequence, which avoids time consuming equidistant sampling along the CS dimension k_ω. The suggested phase encoding scheme is combined with a reconstruction algorithm that exploits prior knowledge about the chemical shifts of the resonances present in the sample under investigation. To provide the resonance frequencies, an additional single voxel experiment must be carried out to obtain the chemical shift of water, unless it is already known from previous studies. Efficient water and lipid suppression is a prerequisite for the application of the method to proton SI to make sure that metabolite signals are free from severe signal interferences. A reference experiment for acquiring the unsuppressed water signal has to be carried out to correct for effects of B_0 inhomogeneities.

The results of this study confirm the applicability of adjusted chemical shift phase encoding for ^{1}H spectroscopic U-FLARE imaging. In phantom and *in vivo* experiments, signals of all metabolites that can be reconstructed by conventional Fourier transformation followed by peak integration can also be reconstructed by the APE method. However, APE can be applied to only one quarter of the data set instead of using the full set of 64 CS phase encoding steps as in the conventional method. Both methods provide similar image quality and *SNR* per unit measuring time if the subset of phase encoding steps is chosen appropriately. In contrast to the conventional method, how-

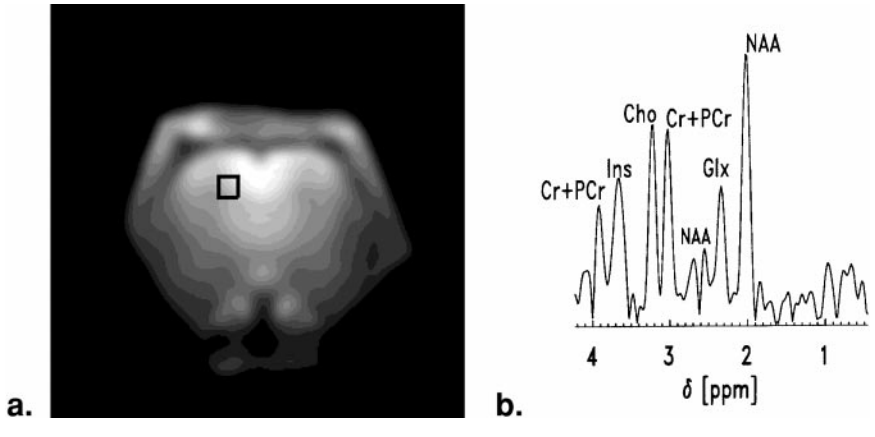

FIG. 6. (a) MRI image from the rat brain: The same slice was selected for the spectroscopic U-FLARE experiment. The black square marks the position of the voxel, for which the magnitude spectrum is shown in (b) as a typical example.

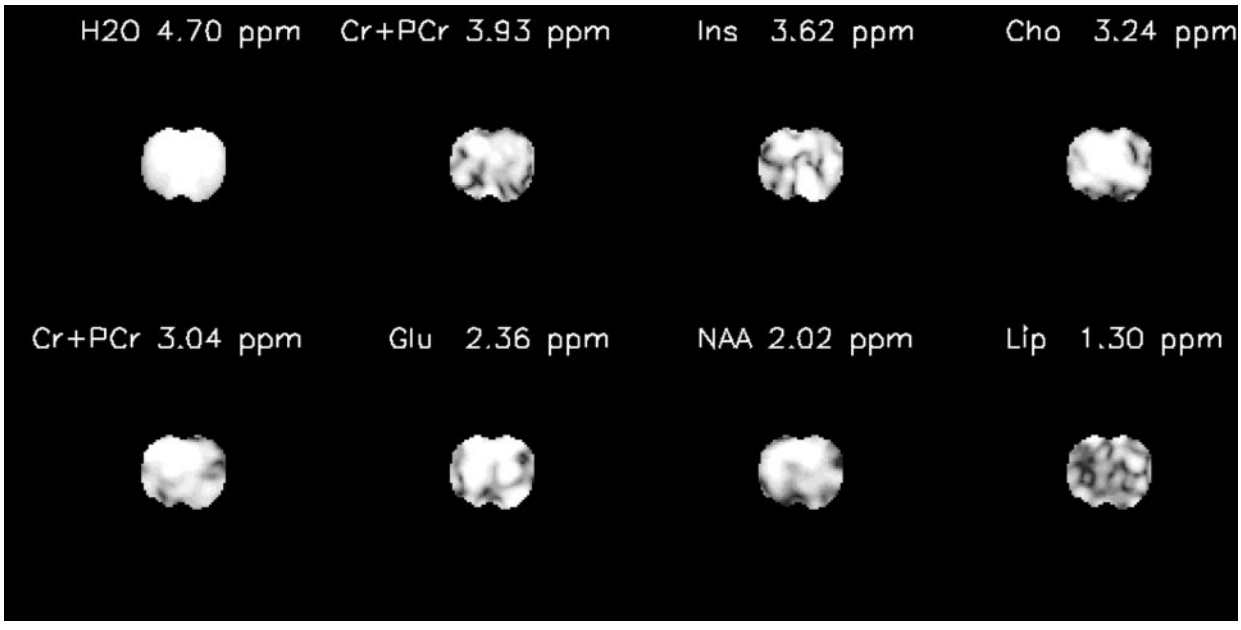

FIG. 7. Spectroscopic U-FLARE images of the rat brain obtained by the conventional Fourier transform method. As in Fig. 4 the water image in the top-left corner was reconstructed from the unsuppressed water reference signal.

ever, APE does not provide spectra for the voxels, which is why this method depends on correct prior knowledge about *all* resonances present. In our experiments, we found that variations of the resonance frequencies in the order of ± 4 Hz had no significant effect on the image reconstruction. Thus, changes of the chemical shift of water across the sample by ± 0.02 ppm at 4.7 T that could be caused by temperature variations by ± 2°C (*48*) can be neglected. Using the APE method, the additional measuring time necessary for *SNR* enhancement could be used for spatial phase encoding along the third dimension k_z, for example. The reference experiment, which, in principle, does not necessarily have to be performed for the conventional reconstruction method, does not significantly increase the total duration of an experiment. In a longer series of (multidimen-

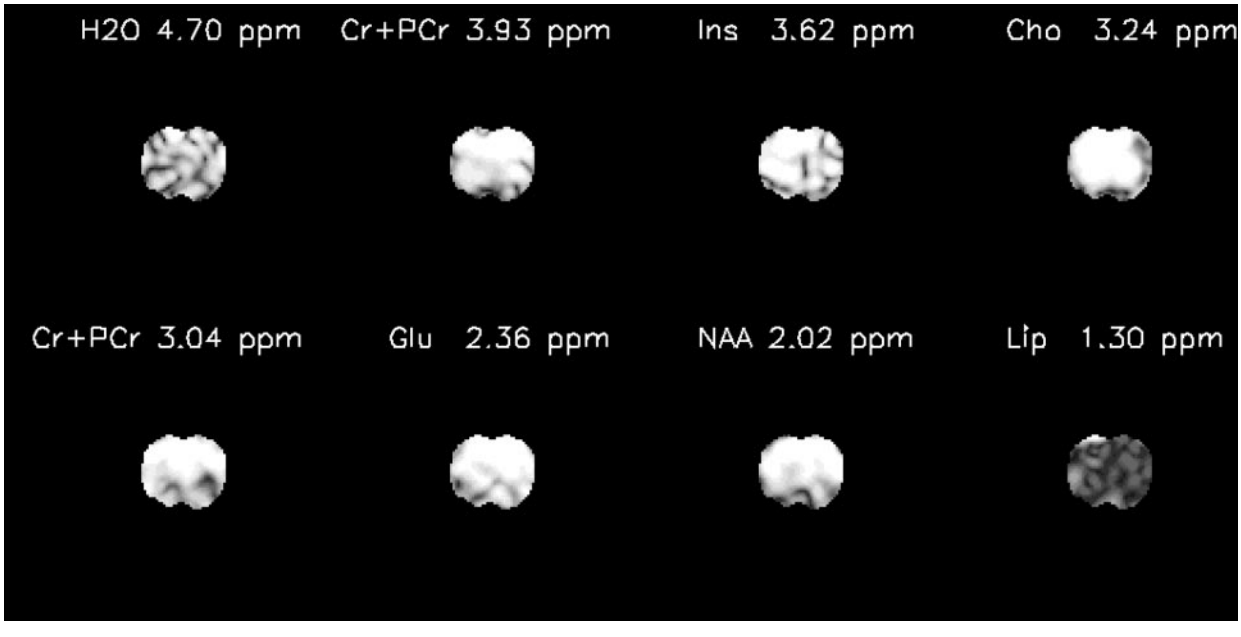

FIG. 8. Metabolic maps of the rat brain calculated with the APE algorithm using a selection of 16 out of the total of 64 CS phase encoding steps. As in Fig. 5, the water image in the top-left corner was reconstructed from the same data as the images of the other metabolites.

sional) measurements, the time needed for the reference measurement is short compared to the duration of the whole experiment.

The influence of noise and signal instabilities on the APE reconstruction can be controlled by appropriately adjusting the CS phase-encoding times. The metabolite signals to be reconstructed with the APE method will be liable to signal leakage depending on how the matrix B^+ in Eq. [3] is conditioned. Signal separation may become imperfect, and the images will show a superposition of contributions from different resonances. A measure of the condition of B^+ is given by its matrix norm $\|B^+\|$ (cf. Eq. [6]), which is the factor of proportionality connecting the standard deviation of noise (and other random signal fluctuations) in the measured signals with that in the reconstructed signals. Therefore, the choice of CS phase-encoding times should aim to minimize this quantity in order to render the APE algorithm as robust as possible. As the effect of B_0 inhomogeneities on the shape of the pseudo-echo in k_ω is not known a priori and may vary across the sample, assumptions with respect to the attenuation factors $|f(\tau_j)|$ must be considered, e.g., an exponential decay with an estimated effective decay constant T^{**}_2.

As for APE in contrast to the conventional FT method there is no general restriction on the range of encoding times $T_t \equiv \max_j(\tau_j) - \min_j(\tau_j)$, the adjustment of the phase encoding times can also aim to reduce this quantity. Apart from reducing signal attenuation due to B_0 inhomogeneities, this will allow the choice of shorter evolution periods *tc* optimized for the detection of specific coupled nuclei. Furthermore, signal loss due to T_2 relaxation during *tc* will be reduced. Limitations of the APE method mainly arise from signal instabilities due to motion or flow or from frequency variations across the sample due to temperature gradients. Thus, the reduction of the minimum total measuring time achieved by APE should preferably be exploited for applications with 3D spatial resolution rather than for dynamic studies.

REFERENCES

1. T. R. Brown, B. M. Kincaid, and K. Ugurbil, NMR chemical shift imaging in three dimensions, *Proc. Natl. Acad. Sci. USA* **79,** 3523–3526 (1982).
2. A. A. Maudsley, S. K. Hilal, W. H. Perman, and H. E. Simon, Spatially resolved high resolution spectroscopy by "four-dimensional" NMR, *J. Magn. Reson.* **51,** 147–152 (1983).
3. P. Mansfield, Spatial mapping of the chemical shift in NMR, *J. Phys. D: Appl. Phys.* **16,** L235–L238 (1983).
4. P. Mansfield, Spatial mapping of the chemical shift in NMR, *Magn. Reson. Med.* **1,** 370–386 (1984).
5. A. Macovski, Volumetric NMR imaging with time-varying gradients, *Magn. Reson. Med.* **2,** 29–40 (1985).
6. S. Matsui, K. Sekihara, and H. Kohno, High-speed spatially resolved NMR spectroscopy using phase-modulated spin-echo trains. Expansion of the spectral bandwidth by combined use of delayed spin-echo trains, *J. Magn. Reson.* **64,** 167–171 (1985).
7. S. Matsui, K. Sekihara, and H. Kohno, High-speed spatially resolved high-resolution NMR spectroscopy, *J. Am. Chem. Soc.* **107,** 2817–2818 (1985).
8. S. Matsui, K. Sekihara, and H. Kohno, Spatially resolved NMR spectroscopy using phase-modulated spin-echo trains, *J. Magn. Reson.* **67,** 476–490 (1986).
9. I. L. Pykett and R. R. Rzedzian, Instant images of the body by magnetic resonance, *Magn. Reson. Med.* **5,** 563–571 (1987).
10. D. G. Norris and W. Dreher, Fast proton spectroscopic imaging using the sliced *k*-space method, *Magn. Reson. Med.* **30,** 641–645 (1993).
11. J. Frahm, H. Bruhn, M. L. Gyngell, K. D. Merboldt, W. Hänike, and R. Sauter, Localized proton NMR spectroscopy in different regions of the human brain *in vivo.* Relaxation times and concentrations of cerebral metabolites, *Magn. Reson. Med.* **11,** 47–63 (1989).
12. A. Allerhand, Analysis of Carr–Purcell spin-echo NMR experiments on multiple-spin systems. The effect of homonuclear coupling, *J. Chem. Phys.* **44,** 1–9 (1966).
13. R. M. Henkelman, P. A. Hardy, J. E. Bishop, C. S. Poon, and D. B. Piewes, Why fat is bright in RARE and fast spin-echo imaging, *J. Magn. Reson. Imaging.* **2,** 533–540 (1992).
14. W. Dreher and D. Leibfritz, Improved proton spectroscopic U-FLARE imaging for the detection of coupled resonances in the rat brain *in vivo, Magn. Reson. Imaging.* **17,** 611–621 (1999).
15. A. Bax and R. Freeman, Investigation of complex networks of spin–spin coupling by two-dimensional NMR, *J. Magn. Reson.* **44,** 542–561 (1981).
16. W. Dreher and D. Leibfritz, Detection of homonuclear decoupled *in vivo* proton NMR spectra using constant time chemical shift encoding: CT-PRESS, *Magn. Reson. Imaging.* **17,** 141–150 (1999).
17. G. C. Danielson and C. Lanczos, Some improvements in practical Fourier analysis and their application to X-ray scattering from liquids, *J. Franklin Institute* **233,** 365–380; 435–452 (1942).
18. J. W. Cooley and J. W. Tukey, An algorithm for the machine calculation of complex Fourier series, *Math. Comput.* **19,** 297–301 (1965).
19. C. E. Shannon, Communication in the presence of noise, *Proc. IRE* **37,** 10–21 (1949).
20. J. L. Ackerman, J. Koutcher, and T. J. Brady, Minimal sampling of the free induction decay: Applications to high speed chemical shift imaging and multidimensional spectroscopy, *in* "Proc., SMRM, 4th Annual Meeting, London, 1985," p. 133.
21. J. W. C. van der Veen, R. de Beer, P. R. Luyten, and D. van Ormondt, Accurate quantification of *in vivo* ^{31}P NMR signals using the variable projection method and prior knowledge, *Magn. Reson. Med.* **6,** 92–98 (1988).
22. S. Y. Kung, K. S. Arun, and D. V. Bhaskar Rao, State space singular value decomposition based methods for the harmonic retrieval problem, *J. Opt. Soc. Am.* **73,** 1799–1811 (1983).
23. Y. Hiltunen, M. Ala-Korpela, J. Jokisaari, S. Eskelinen, K. Kiviniitty, M. Savolainen, and Y. A. Kesäniemi, A lineshape fitting model for ^{1}H NMR spectra of human blood plasma, *Magn. Reson. Med.* **21,** 222–232 (1991).
24. S. W. Provencher, Estimation of metabolite concentrations from localized *in vivo* NMR spectra, *Magn. Reson. Med.* **30,** 672–679 (1993).
25. R. Brüschweiler, J. C. Madsen, C. Griesinger, O. W. Sørensen, and R. R. Ernst, Two-dimensional NMR spectroscopy with soft pulses, *J. Magn. Reson.* **73,** 380–385 (1987).

26. G. Strang. "Linear Algebra and Its Applications," Harcourt Brace Jovanovich, San Diego (1988).

27. W. T. Dixon, Simple proton spectroscopic imaging, *Radiology* **153,** 189–194 (1984).

28. G. H. Glover and E. Schneider, Three-point Dixon technique for true water/fat decomposition with B_0 inhomogeneity correction, *Magn. Reson. Med.* **18,** 371–383 (1991).

29. A. M. Mood and F. A. Graybill. "Introduction to the Theory of Statistics," McGraw–Hill, New York (1963).

30. A. Ebel. "Schnelle ^{1}H-NMR-spektroskopische Bildgebung mittels angepaßter Phasenkodierung der chemischen Verschiebung," Ph.D. thesis, Universität Bremen (1999).

31. P. Börnert and W. Dreher, Chemical-Shift selective NMR imaging using adjusted phase encoding, *J. Magn. Reson.* **87,** 220–229 (1990).

32. J. A. Nelder and R. Mead, A simplex method for function minimization, *Comp. J.* **7,** 308–313 (1965).

33. R. J. T. Corbett, A. R. Laptook, G. Tollefsbol, and B. Kim, Validation of a noninvasive method to measure brain temperature *in vivo* using ^{1}H NMR spectroscopy, *J. Neurochem.* **64,** 1224–1230 (1995).

34. P. Webb, D. Spielman, and A. Macovski, Inhomogeneity correction for *in vivo* spectroscopy by high-resolution water referencing, *Magn. Reson. Med.* **23,** 1–11 (1992).

35. A. A. de Graaf, J. E. van Dijk, and W. M. M. J. Bovée, QUALITY: Quantification improvement by converting lineshapes to the Lorentzian type, *Magn. Reson. Med.* **13,** 343–357 (1990).

36. G. A. Morris, Compensation of instrumental imperfections by deconvolution using an internal reference signal, *J. Magn. Reson.* **80,** 547–552 (1988).

37. A. A. Maudsley, Spectral lineshape determination by self-deconvolution, *J. Magn. Reson. B* **106,** 47–57 (1995).

38. C. T. W. Moonen, ^{1}H MRS of the Brain, *in* "ISMRM Syllabus," p. 184, ISMRM, Berkeley (1994).

39. D. J. Lurie, A systematic design procedure for selective pulses in NMR imaging, *Magn. Reson. Imaging.* **3,** 235–243 (1985).

40. Z. Starčuk and V. Sklenář, New hard pulse sequences for the solvent signal suppression in Fourier-transform NMR. II, *J. Magn. Reson.* **66,** 391–397 (1986).

41. J. Mao, T. H. Marcel, and E. R. Andrew, Experimental study of optimal selective 180° radiofrequency pulses, *J. Magn. Reson.* **79,** 1–10 (1988).

42. D. G. Norris and P. Börnert, Coherence and interference in ultrafast RARE experiments, *J. Magn. Reson. A* **105,** 123–127 (1993).

43. D. G. Norris, U. Böttcher, and D. Leibfritz, A simple method of generating variable T1 contrast images using temporally reordered phase encoding, *Magn. Reson. Med.* **15,** 483–490 (1990).

44. "IDL User's Guide," Research Systems, Inc. (1995).

45. E. Anderson, Z. Bai, C. Bischof, J. Demmel, J. Dongarra, J. Du Croz, A. Greenbaum, S. Hammarling, A. McKenney, S. Ostrouchov, and D. Sorensen. "LAPACK Users' Guide," SIAM (1994).

46. K. L. Behar and T. Ogino, Assignment of resonances in the ^{1}H spectrum of rat brain by two-dimensional shift correlated and J-resolved NMR spectroscopy, *Magn. Reson. Med.* **17,** 285–303 (1991).

47. J. Pfeuffer, I. Tkac, S. W. Provencher, and R. Gruetter, Towards an *in vivo* neurochemical profile: Quantification of metabolites in ultrashort echo time ^{1}H MRS of rat brain accounting for macromolecule resonances, *MAG*MA* **6,** 15 (1998).

48. K. Kuroda, K. Oshio, A. H. Chung, K. Hynynen, and F. A. Jolesz, Temperature mapping using the water proton chemical shift: A chemical shift selective phase mapping method, *Magn. Reson. Med.* **38,** 845–851 (1997).